Available online at www.sciencedirect.com

ScienceDirect

Journal of Asian Earth Sciences 29 (2007) 407–423

Journal of Asian Earth Sciences

www.elsevier.com/locate/jaes

A structural transect in the Lower Dolpo: Insights on the tectonic evolution of Western Nepal

R. Carosi [a,b,*], C. Montomoli [a,b], D. Visonà [b,c]

[a] *Università di Pisa, Dipartimento di Scienze della Terra, via S. Maria, 53 56126 Pisa, Italy*
[b] *Istituto di Geoscienze e Georisorse (CNR) via Moruzzi, 1, 56124 Pisa, Italy*
[c] *Università di Padova, Dipartimento di Mineralogia e Petrologia, c.so Garibaldi 37, 35122 Padova, Italy*

Received 31 January 2005; accepted 2 May 2006

Abstract

We present the results of a structural transect in Lower Dolpo, cross-cutting the upper part of the Lesser Himalaya (LH), the Higher Himalayan Crystallines (HHC) and the lower part of the Tibetan Sedimentary Sequence (TSS). The MCT zone affects the upper part of the LH as well as the lower part of the HHC and shows a later brittle reactivation. Mean vorticity in the MCT points to non-coaxial deformation. These data, together with available kinematic data along the belt, on the South Tibetan Detachment System (STDS) and in the core of the HHC, point to increasing simple shear toward the tectonic boundaries. A top-to-the-SW high-temperature shear zone (Toijem Shear Zone) is recognized in the middle part of the HHC at the boundary between Units 1 and 2. It developed during the earlier stages of exhumation of the HHC, enhancing the decompression of the hanging wall and the emplacement of leucogranite dykes and sills. Its development could be explained by a change in the velocity profile during the extrusion of the HHC, triggered by first order changes in rock types of the tectonic unit. The STDS is marked by a wide zone of high strain and by a metamorphic jump from amphibolite facies in the carbonate rocks of the upper part of the HHC to greenschist facies marbles in the lower part of the TSS. The development of a pervasive foliation towards the bottom of the TSS indicates increasing strain, related to top down-to-the-NE tectonic transport. A Low P metamorphic event, marked by the growth of post-D1 biotite porphyroblasts at the base of the TSS, is related to the conductive heating from the underlying HHC.

Keywords: Himalayas; Lower Dolpo; Main Central Thrust Zone; South Tibetan Detachment System; High-temperature shear zones; Tectonic extrusion; Out-of-sequence thrust

1. Introduction

The Himalayan Belt, with its high elevation and the highest mountains in the world developed during India–Asia collision since 50 Ma, is regarded as a classic collisional orogen and has greatly attracted the attention of international researchers since the last century. Some of its particular features, such as the impressive continuity of thrusts and normal faults and large volume of high-grade metamorphic rocks exposed at the surface constitute an invaluable field laboratory for unravelling the mechanisms of exhumation of deep-seated rocks in orogens.

One of the most striking discoveries in the Himalayan Belt in recent years is the presence of normal faults at the top of the Higher Himalayan Crystallines (HHC), contemporaneous with shortening along the Main Central Thrust (MCT) at its base (Burchfiel and Royden, 1985; Burchfiel et al., 1992; Hodges et al., 1993). A system of low-angle normal faults (South Tibetan Detachment System: STDS) has been detected at the top of the HHC in central and eastern Nepal (Caby et al., 1983; Burg et al., 1984; Burchfiel et al., 1992; Brown and Nazarchuk, 1993; Coleman, 1996; Carosi et al., 1998; Godin et al., 1999b).

* Corresponding author. Tel.: +39 050 2215727; fax: +39 050 2215800.
E-mail addresses: carosi@dst.unipi.it (R. Carosi), montomoli@dst.unipi.it (C. Montomoli).

1367-9120/$ - see front matter
doi:10.1016/j.jseaes.2006.05.001

This striking geological feature has led to the development of new models for the exhumation of deep seated metamorphic rocks, ranging from extrusion of the HHC as a rigid wedge, to ductile extrusion, and channel flow (Burchfiel et al., 1992; Hodges et al., 1993; Grujic et al., 1996, 2002: Vannay and Grasemann, 2001; Grasemann et al., 1999; Daniel et al., 2003; Edwards et al., 1996, 1999; Catlos et al., 2004; Law et al., 2004). These models have had consequences for our understanding of the tectonic and metamorphic evolution of the Himalayan Belt, which has helped to clarify the evolution of other ancient and recent orogens (Chemenda et al., 1995).

Notwithstanding its primary role in the comprehension of the tectonic, stratigraphic, metamorphic, and petrologic evolution of collisional orogens, the Himalayan Belt has not yet been completely mapped, and large areas are still poorly known due to the very large extent of the belt and, sometimes, its difficulty of access. For example, the HHC is often regarded as a unitary high-grade crystalline unit with similar tectonic and metamorphic features throughout the Himalayan Belt (Le Fort, 1975) and most researchers have concentrated their studies on the upper and lower tectonic boundaries for their primary role in the exhumation of the unit. However, structural discontinuities, such as shear zones, thrusts and normal faults have been reported within the HHC, with different interpretations, in the exhumation history of the crystalline unit from Bhutan (Davidson et al., 1997; Grujic et al., 2002) to Nepal (Hodges et al., 1996; Macfarlane, 1993; Maruo and Kizaki, 1983; Vannay and Hodges, 1996; Searle, 1999; Goscombe and Hand, 2000).

The aim of this work is to describe the geological and structural features of the main tectonic units (LH, HHC, and TSS) cropping out along a northeast–southwest transect, located in Western Nepal. The superb exposure of the crystalline units in this area allowed the unravelling of their structural and kinematic evolution and the identification of a ductile shear zone in the middle portion of the HHC.

The study area is located in the remote region of Lower Dolpo where up to the 1990s access was closed to foreigners, and even now is not easy (Fig. 1). Our geological transect starts from Jumla and cuts twice across the three main tectonic units, through the Kangmara La (pass) and the Phoksundo Tal (lake) and ends at Dunai (Fig. 1). The extensive mapping and work of Fuchs (1964, 1977) and Fuchs and Frank (1970), in the 60s and in the 70s constituted an invaluable source of information.

2. Geological setting

From south to north in the Nepal Himalayas the transect passes from the more external areas of the chain towards the higher peaks to the north (Gansser, 1964; Le Fort, 1975; Upreti, 1999 with references therein) where the following tectonic-geomorphologic zonation can be observed (Fig. 1):

1. The Siwalik Hills, bordering the Ganges plain, made up of Himalayan foreland basin sediments of Miocene to Pliocene–Pleistocene age;

2. Lesser Himalayas (LH), including the Mahabharat Range and the Midland zone, is bounded to the south by the Main Boundary Thrust (MBT) and to the north by the Main Central Thrust (MCT). The Lesser Himalayas consists of a thick sequence of weakly metamorphosed sediments (Precambrian to Eocene) and higher-grade metamorphic rocks (Lower Himalayan Crystalline Nappes; Fuchs and Frank, 1970), which overlie the low-grade metasediments. The contact between LH and the overlying HHC, mapped by Fuchs and Frank (1970) broadly corresponds with the Ramgarh Thrust (DeCelles et al., 2001; Robinson et al., 2003).

3. Higher Himalayas, north of the Lesser Himalayan zone, are made up of thrust sheets of metamorphic rocks dipping gently to the north, the Higher Himalayan Crystallines (HHC) and the overlying Tethyan Zone; Miocene leucogranite plutons occur at the boundary between the metamorphic and sedimentary sequences (Fig. 1);

4. Further north, between the main peaks and the Indus Tsangpo Suture Zone, the mountain ranges of the Tibetan Plateau consist of folded Tethyan marine sediments deposited on the north Indian continental paleo-margin. The southern Tethyan sediments are a fossiliferous sequence of Cambrian-Early Ordovician to Eocene age (Mu et al., 1973; Bureau of Geology and Mineral Resources of Xizang Autonomous Region, 1993; Garzanti, 1999; Upreti, 1999 with references). A sequence of metasedimentary rocks of low metamorphic grade (metasandstone, phyllite, quartzite and metalimestone) occurs between the southern Tethyan fossiliferous sequence and the underlying HHC. The Cambrian (?) – Ordovician Dhaulagiri Limestone represents the lower part of the Tethyan sediments in Dolpo region.

High-level plutons of biotite-muscovite granite, the North Himalayan granites, were emplaced during the Miocene in gneiss domes constituting the core of the North Himalayan antiform (Hodges, 2000) and in the overlying Triassic Tethyan sediments (Watts and Harris, 2005).

3. Lesser Himalaya

The Lesser Himalaya has been divided into a lower Lesser Himalayan Sequence, characterized by sediments and very low metamorphism, and an upper crystalline unit, the Lesser Himalayan Crystallines (LHC), consisting of low-grade metamorphic rocks (Fuchs and Frank, 1970) reaching lower amphibolite facies in the uppermost portion. The upper portion of the Lesser Himalaya cropping out in the study area is the Chail Nappe 3 of Fuchs and Frank (1970) or the Upper Nawakot unit (Upreti, 1999 with references therein).

The LHC is represented by phyllites, quartzites, kyanite-bearing quartzites, amphibolites, and micaschists (Fig. 2).

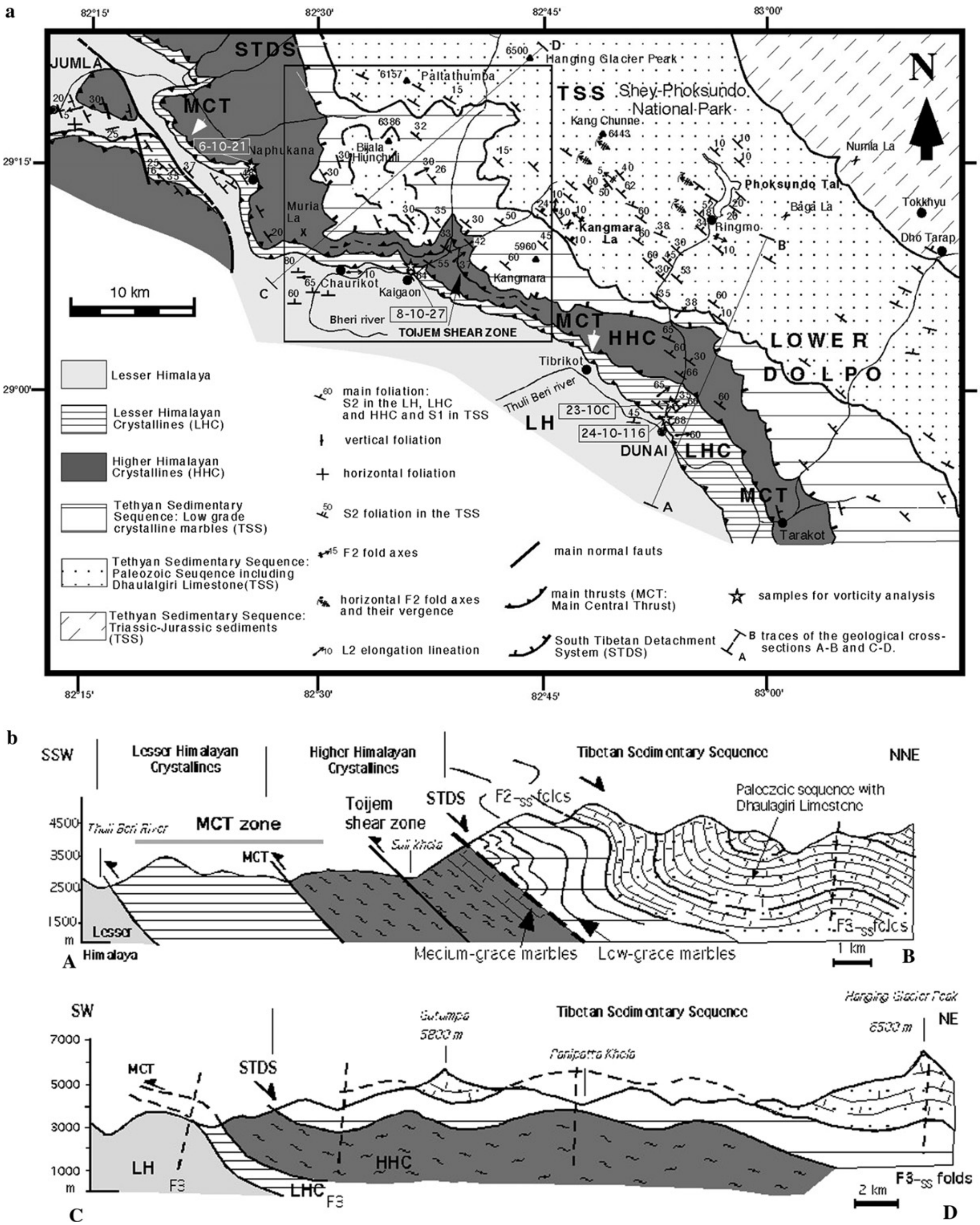

Fig. 1. (a) Geological sketch map of the Dolpo area (from Fuchs, 1964; Fuchs and Frank, 1970; Carosi et al., 2002 modified). 1. Lesser Himalaya; 2. Lesser Himalaya Crystallines (LHC); 3. Higher Himalayan Crystallines; 4. low-grade crystalline marbles (TSS); 5. Paleozoic sequence including Dhaulagiri Limestone (TSS); 6. Triassic-Jurassic sediments (TSS); 7. main foliation (S2 in the LH, LHC, and HHC and S1 in TSS); 8. vertical foliation; 9. horizontal foliation; 10. S2 foliation in the TSS; 11. F2 fold axes; 12. horizontal F2 fold axes and their vergence; 13. L2 elongation lineation; 14. main normal faults; 15. main thrusts (MCT: Main Central Thrust); 16. detachment (STDS: South Tibetan Detachment System); 17. samples for vorticity analysis; 18. traces of the geological cross-sections (A–B) and (C–D); The box indicates the area shown in Fig. 7; (b) Geological cross-sections (A–B) (modified after Carosi et al., 2002) and (C–D). Section (C–D) highlights the presence of NW–SE trending upright F3 antiforms and synforms affecting all the tectonic units.

The metamorphic assemblage of pelites is Qtz + Pl + Bt + Ms + Grt ± St ± Ky ± Chl with accessory tourmaline, zircon, apatite, titanite, and clinozoisite (abbreviations after Kretz, 1983).

According to Fuchs and Frank (1970) the LHC comprises phyllites, micaschists, gneisses, quartzites, and amphibolites, metamorphosed under greenschist facies, reaching the garnet-zone. We found staurolite relics in

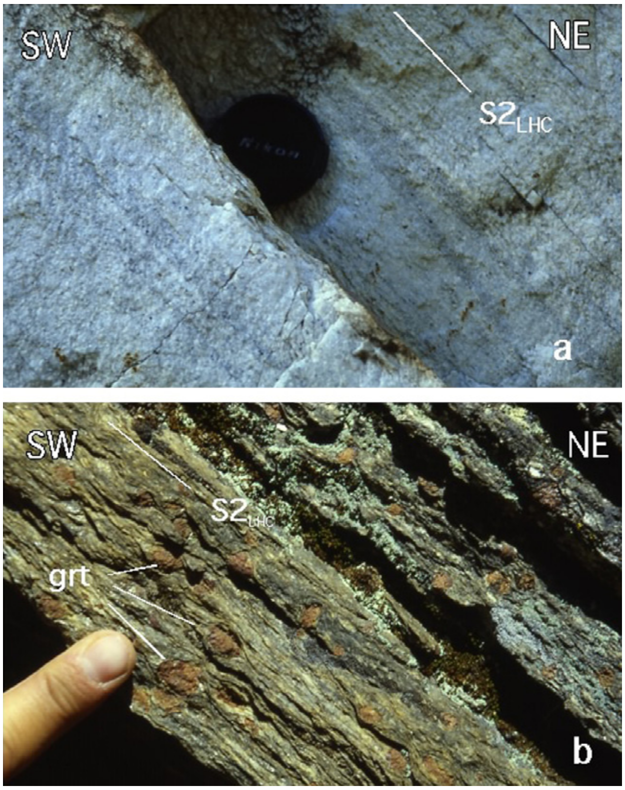

Fig. 2. Kyanite-bearing white quartzites (a) and garnet-bearing micaschists (b) in the LHC near Napukana village. $S2_{LHC}$ is the main foliation in the LHC lithotypes.

garnet-bearing micaschist and kyanite in the white quartzites in the upper portion (Fig. 2) pointing to lower amphibolite facies metamorphism.

In the LHC, an inverted metamorphic field gradient from greenschist to lower amphibolite facies has been observed in the study area, in accordance with observations in other parts of the orogen (Le Fort, 1975; Arita, 1983; Upreti, 1999 and references therein; Hodges, 2000 and references therein).

Two main phases ($D1_{LHC}$ and $D2_{LHC}$) of deformation have been recognized in the Lesser Himalayan Crystallines (LHC). The prominent foliation at outcrop and microscopic scales is an $S2_{LHC}$ foliation, transposing an earlier $S1_{LHC}$ foliation. Relics of the earlier $S1_{LHC}$ foliation are recognized as inclusion trails in plagioclase and garnet porphyroblasts and microlithons between $S2_{LHC}$ foliation surfaces. The $S2_{LHC}$ foliation in the LHC presents mylonitic characteristics with a NW–SE striking foliation, dipping moderately to the NE (Fig. 3). The $L2_{LHC}$ lineation, marked by elongated quartz and tails around porphyroclasts, trends NE–SW and plunges both to the NE and SW (Fig. 3).

Shear band cleavage (Passchier and Trouw, 1996), mica fish, foliation fish, and rotated garnet porphyroblasts are common in the more strained areas. $F2_{LHC}$ tight to isoclinal folds are also present. Kinematic indicators show always a top-to-the-SW sense of shear (Fig. 4).

Two later phases of deformation, with axes trending roughly NW–SE and NE–SW, affect the $S2_{LHC}$ foliation (Fig. 5). The folds vary from open to chevron folds with steeply dipping to sub-vertical axial planes. At the microscopic scale a sub-vertical spaced crenulation cleavage affects the $S2_{LHC}$ fabric.

Low-angle shear zones are common in the upper part of the LH with a top-down to the SW and W sense of displacement. They are ductile/brittle to brittle and overprint the main fabric in the LH. Between Jumla and Depalgaon villages (Fig. 1), cm- to dm-size C-S and C′ fabrics are present in mylonites derived from quartzites and phyllites. The boundaries of the shear zones are parallel to sedimentary bedding. They are top-to-the-south compressional shear zones folded by NW–SE trending later antiforms. So that on the southwestern folds limb they show a normal sense of movement. Similar structures have been described further west by DeCelles et al. (2001).

4. Main Central Thrust Zone

The Main Central Thrust corresponds to a thick zone (nearly 1–4 km) of penetrative mylonitic deformation affecting both the HHC and the LHC. It is almost impossible to identify a single tectonic surface or a narrow high-strain zone corresponding to the MCT because, as observed already by other authors (Arita, 1983; Upreti, 1999; Paudel and Arita, 2000; Catlos et al., 2002; Takagi et al., 2003), there is no a sharp jump in deformation and metamorphic grade between the lower part of the HHC and the upper part of the LHC (Vannay and Hodges, 1996). In fact, both the lower part of the HHC and the upper part of the LHC (if not all the LHC) have been transformed into mylonites with the same top-to-the-SW kinematics (Figs. 4 and 6). The MCT zone corresponds to a high-strain zone (Fig. 7) characterized by mylonites with various types of kinematic indicators, both at the outcrop and the microscopic scale (Fig. 8), according to the definition proposed by Searle and Godin (2003). It affects the lower part of HHC (kyanite and sillimanite bearing gneisses) and the middle and upper portion of LHC (white quartzites, marbles, amphibolites, paragneiss, micaschists, and phyllites; Fuchs and Frank, 1970). A similar interpretation of the MCT zone has been proposed in Langtang by Takagi et al. (2003).

However, within the MCT zone it is possible to observe a lithological change from kyanite- and sillimanite-bearing mylonitic gneisses, attributed to the HHC, to lower quartzites, marbles, amphibolites, micaschists, and phyllites, corresponding to the LHC, described and mapped by Fuchs and Frank (1970). This boundary has been mapped as the MCT in Figs. 1 and 7. In this case our MCT zone is slightly different from the ductile MCT zone proposed by Arita (1983), Paudel and Arita (2002), Catlos et al. (2002), Robinson et al. (2003), because these authors confine it to only the LHC.

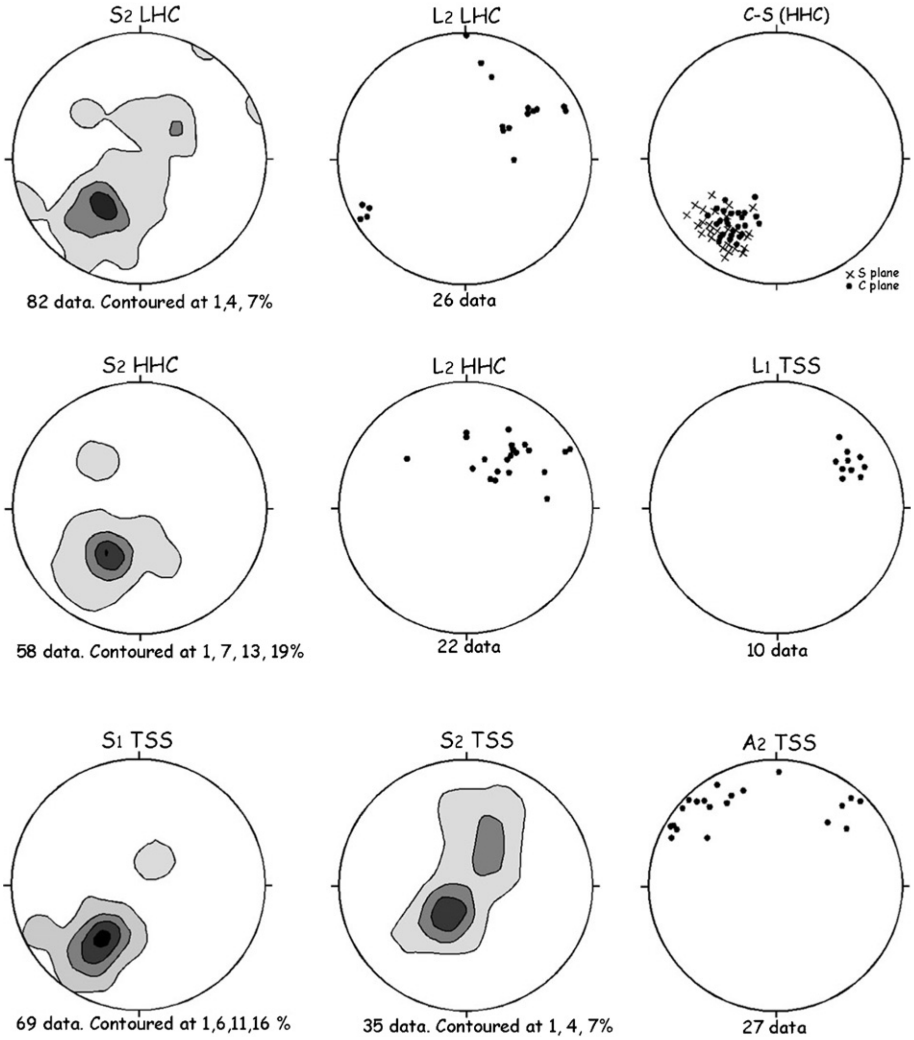

Fig. 3. Stereographic projections of the main structural elements in the LHC, HHC and TSS. S1, first phase foliation; S2, second phase foliation; L1, first phase elongation lineation; L2, second phase elongation and mineral lineation; C-S, C-S fabrics in the HHC; A2, F2 folds axes.

Fig. 4. Mica fish showing a top-to-the SW sense of shear in kyanite-bearing white quartzites in the LHC; CP, field of view is 6 mm.

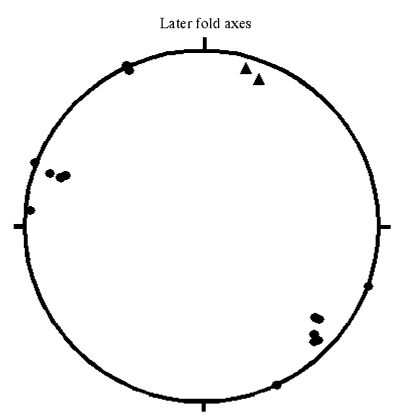

Fig. 5. Stereographic projections of later fold axes: $A3_{LHC}$ (black dots) and $A4_{LHC}$ (black triangles) affecting the $S2_{LHC}$ foliation in the LHC (lower hemisphere).

Well-developed kinematic indicators in the MCT zone are observable few hundred meters NE of Kaigaon, in the upper Bheri river valley (Fig. 8), where C-S fabrics are developed at cm- to dm- scale in phyllites and micaschists (Fig. 6).

In the Suli Khola valley, few hundred meters south of Roha village (Fig. 1), within well-developed mylonites,

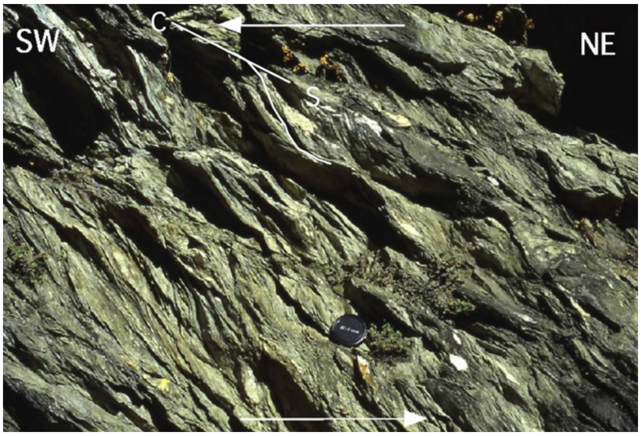

Fig. 6. Examples of C-S fabric in phyllites in the Main Central Thrust zone related to a top-to-the SW sense of shear. North of Kaigaon village.

we can observe a sudden change in the lithologies involved in the shear zone from migmatitic gneiss and kyanite-bearing gneiss in the upper portion (attributed to the HHC) to a complex made up of garnet-bearing micaschists, white quartzites, amphibolites, paragneisses, and phyllites attributed to the LHC. We found biotite, garnet, staurolite, and kyanite in the upper portion of the LHC. A similar sequence was observed at the same structural level few hundred meters west to Napukana village (Fig. 1).

Kinematic indicators are represented by asymmetric folds, rotated porphyroclasts (e.g., garnet), asymmetric pressure shadows and, moreover, by shear band cleavage (Figs. 4, 8). Rootless isoclinal folds are observed in the more strained zones. Shear planes strike N110–120° and dip moderately to steeply to the NE; an elongation lineation trends N40–50° and plunges 50–60° to the NE.

In the MCT zone, an inverted metamorphic field gradient has been confirmed, both at the meso- and micro-scale. Minerals such as biotite, garnet, staurolite, and kyanite are found progressively upward in the sequence. The metamorphic minerals are deformed in the mylonites that show a low-grade metamorphic re-equilibration. Kyanite is bent and sometimes stretched with open spaces filled by muscovite and quartz (Fig. 9).

Brittle/ductile shear zones, overprinting the main ductile fabric (S2), have been recognized near Chaurikot and in the southern part of Suli Khola, approaching the MCT zone (Figs. 1 and 10). They are associated with centimeter to decimeter thick cataclasites and drag folds pointing to a top-to-the W and SW sense of shear. Near Kaigaon foliated cataclasites are associated with shear planes and Riedel shears and drag folds crosscut mylonites of the MCT in phyllites and metabasites. These compressive brittle structures have the same sense of transport as the ductile fabric, and they could represent a later compressive reactivation of the MCT zone in more recent times, after the main ductile phase at upper structural levels (e.g., late Miocene; Macfarlane, 1993; Harrison et al., 1997; Catlos et al., 2002).

4.1. Vorticity analysis

Vorticity analysis was carried out to investigate the degree of non-coaxiality of the flow during deformation (Passchier, 1987; Wallis, 1992, 1995; Wallis et al., 1993; Law et al., 2004). In steady state progressive deformation, ductile shear zones can develop as a result of pure and simple shear components of deformation acting simultaneously.

The degree of non-coaxiality of the flow can be expressed by a mean kinematic vorticity number (W_m, Passchier, 1987) that describes the bulk rotation of material lines coincident with the principal strain axes (W_m is the ratio between the mean angular velocity of lines and the stretching rates). In a pure shear-dominated deformation the kinematic vorticity number (W_m) is zero, while it is one in the case of simple shear deformation. The two components, pure and simple shear, give an equal contribution to the instantaneous flow at $W_m = 0.71$ (Law et al., 2004).

In this work, the mean kinematic vorticity number (W_m) has been estimated following the method proposed by Passchier (1987) and Wallis et al. (1993). This method is based on measuring the orientation (θ) and the aspect ratio ($R = R_{max}/R_{min}$) of rigid porphyroclasts rotating in a surrounding matrix until they reach a stable orientation corresponding to a critical aspect ratio (R_c). Porphyroclasts with an aspect ratio lower than the critical value (R_c) rotate continuously in the matrix, while those with an aspect ratio higher than R_c reach a stable orientation (Ghosh and Ramberg, 1976). The R_c values are linked to vorticity (W_m) by the following relation:

$$W_m = (R_c^2 - 1)/(R_c^2 + 1) (\text{Wallis et al., 1993})$$

Analyses were done on four suitable samples (Fig. 11; Table 1), from the MCT zone (Fig. 1).

Samples 8-10-27 and 24-10-116 are fine grained plagioclase-bearing schist. Samples 6-10-21 and 23-10c are, respectively, a garnet–staurolite–kyanite micaschist and a garnet–muscovite micaschist. All samples are affected by a mylonitic foliation marked by quartz, biotite, muscovite, and chlorite.

Measurements were conducted on thin sections cut parallel to the elongation lineation and perpendicular to the foliation. This was so that they could well-approximate the *XZ* plane of the finite strain ellipsoid, perpendicular to the vorticity vector in a monoclinic shear zone.

The most suitable minerals are plagioclase feldspar porphyroclasts. We selected isolated and non-fractured porphyroclasts coarser than the surrounding matrix. For each sample from 69 to 162 measurements were collected and the axial ratio values (R_{max}/R_{min}), against the orientation of R_{max} with respect to the mylonitic foliation, were plotted in order to estimate the R_c values (Fig. 11; Table 1). We evaluated the minimum and the maximum R_c value according to the distribution of the points on the graph, delimiting the area showing a dispersion of long axes orientation between −90° and +90° from the area showing an

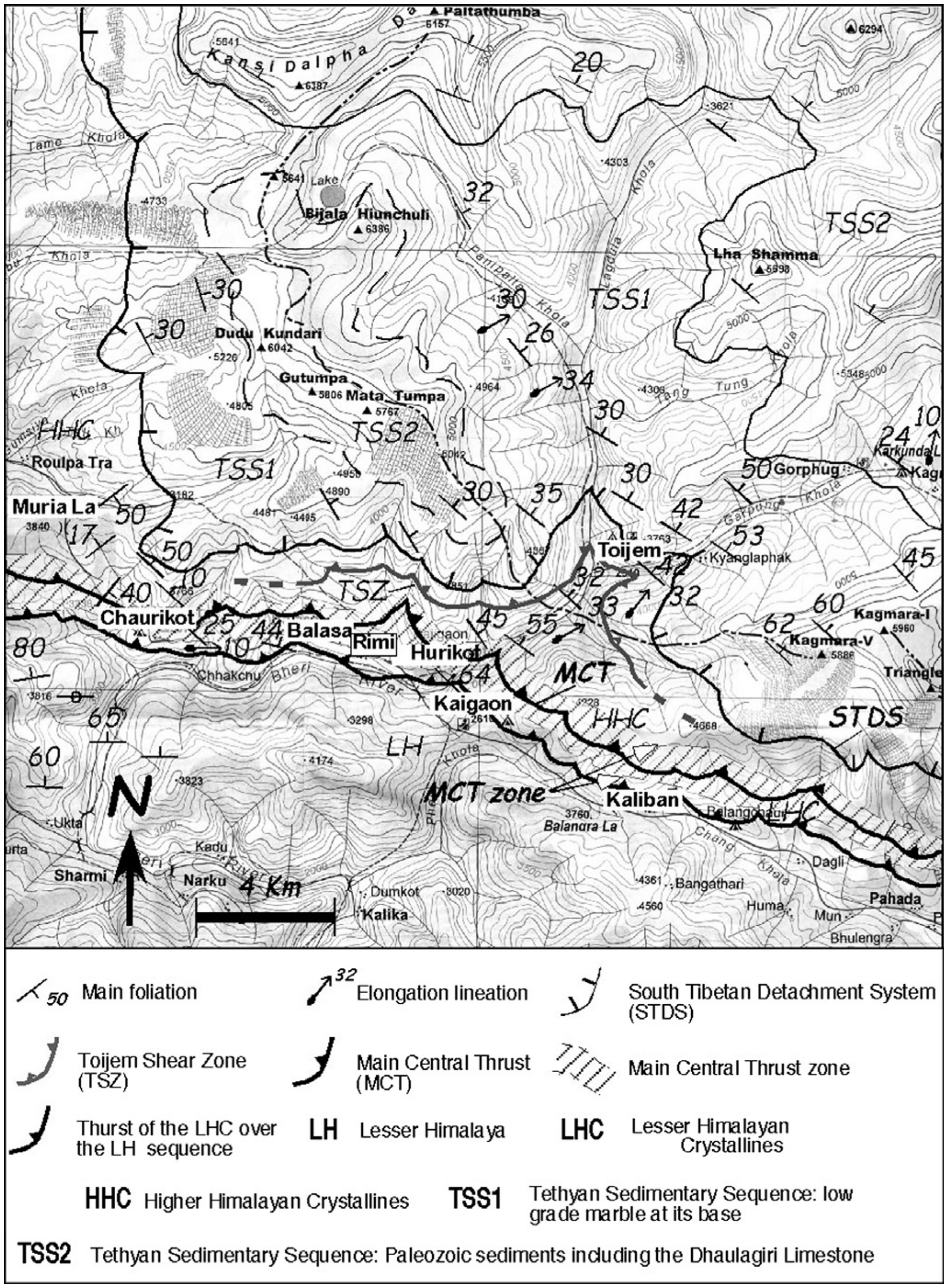

Fig. 7. Geological structural map of the Lower Dolpo area west of Kangmara Peak (after Fuchs and Frank, 1970 and authors' personal work). Topographic map from Nepa Maps by P. Gondoni, scale 1:135.000.

increasing preferred orientation (with decreasing dispersion of long axes orientation angles). There are some uncertainties in evaluating R_c by this method and following Law et al. (2004) we chose the minimum and the maximum R_c estimates and calculated the mean value (Fig. 11; Table 1).

The estimated mean kinematic vorticity number (W_m) varies between 0.66 and 0.77. However, as already noted by Law et al. (2004) rotating clasts with low aspect ratio result in an underestimate the vorticity values. This implies that our mean values can be considered as a minimum estimation of the vorticity of the flow in MCT zone.

These results point to a non-coaxial deformation ranging from pure shear to simple shear component, but close to the boundary between simple and pure shear components ($W_m = 0.71$). They are in good agreement with the vorticity values obtained by Grasemann et al. (1999) in the MCT zone of NW Himalaya.

5. Higher Himalayan Crystallines

The lowest part (Unit 1 of Searle and Godin, 2003 or Formation 1 of Le Fort, 1971) is composed of kyanite

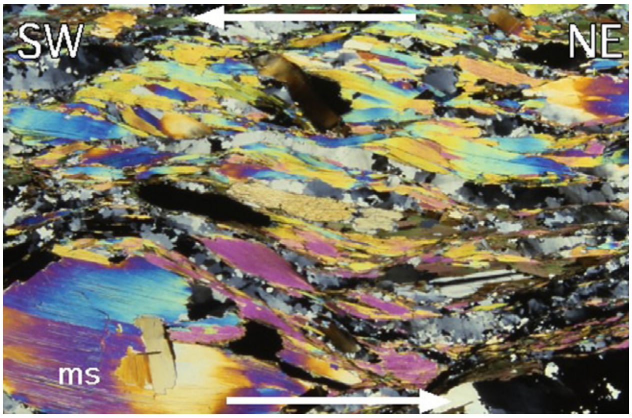

Fig. 8. Mica fish and shear bands in gneisses from the lower part of Unit 1 between Napukana village and Muria La (pass); top-to-the SW sense of shear; CP, field of view is 6 mm.

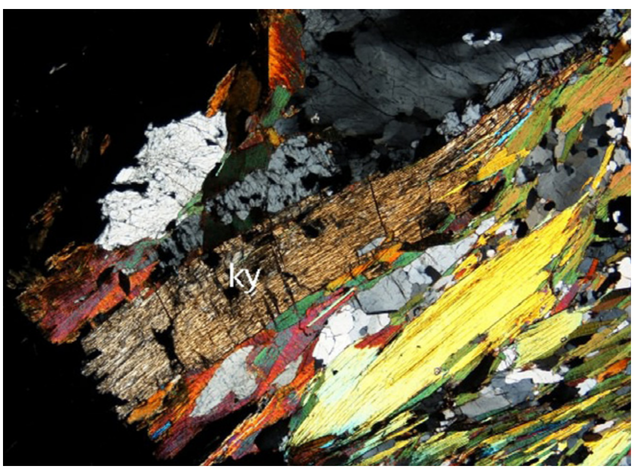

Fig. 9. Kyanite crystals deformed along the $S2_{HHC}$ foliation in the kyanite-bearing gneiss of the HHC; CP; field of view is 5 mm.

(Fig. 12a and b) and garnet-bearing paragneisses and micaschists with thin layers of calc-silicate and boudins of garnet-bearing amphibolite. Abundant cm-size kyanite crystals, sometimes up to 5–6 cm in length, are frequently found. Unit 1 is strongly deformed and it is transformed into mylonite (Fig. 8). The metamorphic stable assemblage in gneisses and micaschists is represented by Qtz + Pl + Bt + Ms + Grt + Ky ± Pl ± St ± Sil with accessory tourmaline, ilmenite, rutile, zircon, apatite, and Fe–Ti oxides. Garnet shows helicitic inclusion trails in the core, with an inclusion free rim. Quartz, staurolite, and paragonite are observed inside garnet crystals. Kyanite and sillimanite porhyroblasts are unstable and armoured by muscovite. Sillimanite has been found in several samples from gneisses of Unit 1 where it occurs as thin and small beards on kyanite crystals, whereas they become abundant at the top of Formation 1 (Gorpung Khola). Sillimanite is elongated parallel to the S2 foliation, around microlithons composed of Ky armoured by Ms (Fig. 12b) or of garnet

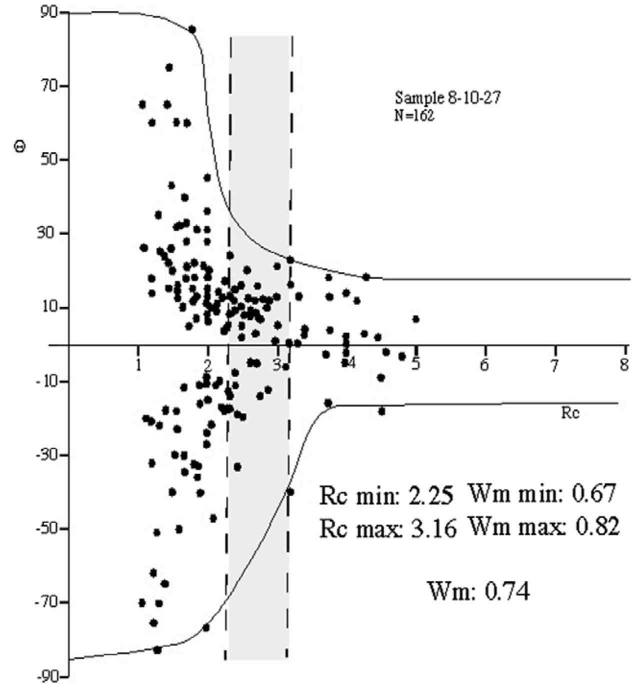

Fig. 11. Example of graph used for vorticity analysis by stable porphyroclast (after Passchier, 1987; Wallis et al., 1993 and Wallis, 1995). R, aspect ratio of porphyroclast; θ, angle between long axis of porphyroclast and foliation; R_c, value of critical aspect ratio; W_m, mean vorticity kinematic number; N, number of measured objects. Grey area indicates the range between the minimum and maximum value of R_c.

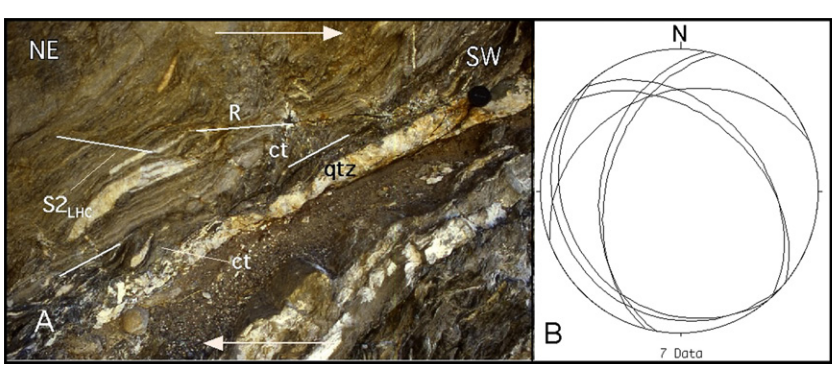

Fig. 10. (A) Brittle reactivation, top-to-SW sense of shear, of the ductile fabric in the MCT zone with development of cataclasites and Riedel synthetic fractures (R); Suli Khola valley. (B) Stereographic projections of brittle shear planes (lower hemisphere).

Table 1
Results of the stable porphyroclast analysis

Sample	N	R_c min	R_c max	R_c m	W_m
8-10-27	162	2.2	3.2	2.7	0.77
24-10-116	132	2.0	3.0	2.5	0.7
6-10-21	69	2.5	3.0	2.75	0.77
23-10-C	115	2.2	2.2	2.2	0.66

Due to uncertainty in calculation of the critical value of R_c, for each section two values of R_c have been reported. R_c min, minimum value of critical aspect ratio; and R_c max, maximum value of critical aspect ratio. N, number of porphyroclasts; R_c m, mean value of critical aspect ratio; W_m, mean value of vorticity.

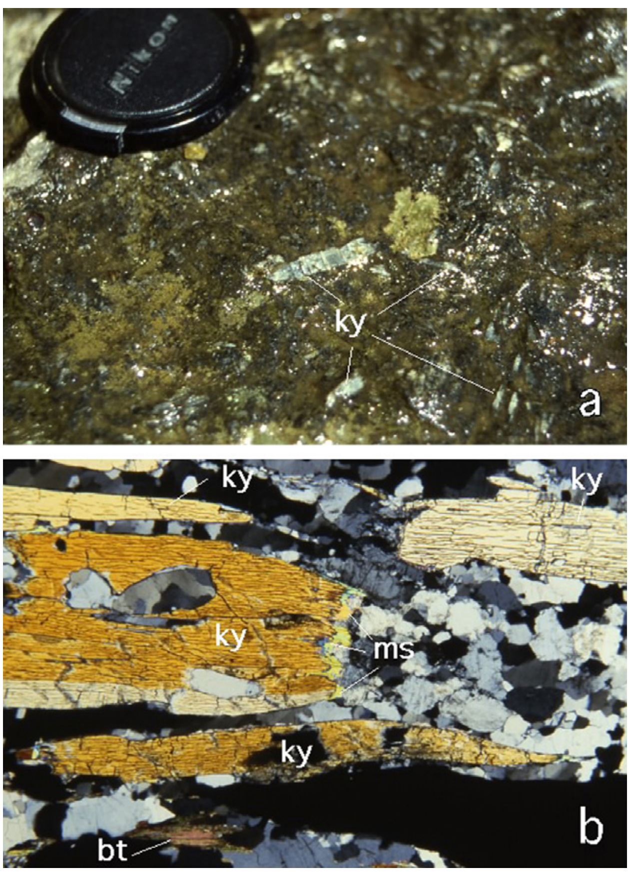

Fig. 12. Unit 1 of the Higher Himalayan Crystallines (HHC). (a) cm-size kyanite (ky) crystals in gneisses (Suli Khola valley; lens cap for scale; diameter 5.2 cm); (b) muscovite (ms) replacing kyanite in kyanite and garnet-bearing gneisses; bt, biotite; Crossed polars; field of view is 1.8 mm (Roha village; Suli Khola valley).

poikiloblasts. Muscovite and biotite are elongated parallel to the foliation and represent a retrograde greenschist facies metamorphism.

Unit 2 (Searle and Godin, 2003 or Formation 2 of Le Fort, 1971) is constituted in Lower Dolpo by few meters of white marbles, calc-silicate gneiss, with minor amounts of pelitic and psammitic rocks follow upward. Eastward, in the Annapurna section, it is several kilometres thick (Vannay and Hodges, 1996).

Few meters, up to some dozen meters, of orthogneiss and migmatite gneiss constitute Unit 3 (Searle and Godin, 2003 or Formation 3 of Le Fort, 1971). Tourmaline-bearing leucogranitic sills and dykes intrude migmatite gneisses. Calc-silicate-bearing marbles make up the top of the sequence; their thickness is nearly 0.5–1 km. Calc-silicate rocks are sometimes intercalated in the gneisses with the assemblage Qtz ± Pl ± Kfs + Cpx + Ep + Scp + Grt + Bt + Ms ± Cc ± Pl ± Hbl with accessory minerals such as tourmaline, rutile, titanite, apatite, zircon, and Fe–Ti oxides (Carosi et al., 2002). The marbles contain the amphibolite facies assemblage of Tr + Cc + Di ± Qtz which is retrogressed to the greenschist facies assemblage of Tr + Cc ± Scap ± Bt ± Qtz.

A network of leucogranite sills and dykes are intruded in the calc-silicates and marbles showing an increasing deformation (from undeformed to stretched and folded) approaching the STD zone. A magnificient exposure of deformed dykes can be observed south of Kangmara and Triangle Peak and on the right side of Panipatta Khola (Figs. 1 and 7). The dykes are several hundred meters long and are tightly folded perpendicularly to the main fabric, and stretched and boudinaged parallel to it. Approaching the STDS they are progressively rotated into parallelism with the main fabric. Similar dykes have been dated at 21.5 Ma by Godin et al. (2001) in the Kali Gandaki.

The thickness of the three units in the HHC is quite variable along the belt and it is highly reduced in the Lower Dolpo section.

The main fabric is a $D2_{HHC}$ shear band cleavage (sensu Passchier and Trouw, 1996). Stretched and fractured kyanite porphyroclasts, quartz, biotite, muscovite, and re-crystallised tails around rigid porphyroclasts mark an elongation and mineral lineation. Preferred orientation of the metamorphic minerals (Bt, Ms, Ky, and Sil) and dynamically re-crystallised quartz mark the main schistosity. In some cases, Ky, St, Ms, and Bt crystals are bent or kinked along shear bands. C-S fabric, shear bands, asymmetric tails around porphyroclasts and rotated garnets constantly indicates a top-to-the SW sense of shear. $S2_{HHC}$ schistosity strikes NW–SE and dips 30–60° toward the NE (Fig. 3).

The $L2_{HHC}$ elongation lineation trends N20–40° and plunges moderately to steeply towards the NE (Fig. 3). An earlier deformation phase is sometimes preserved as relics in $F2_{HHC}$ fold hinges, in $S2_{HHC}$ microlithons and as internal foliation in porphyroblasts.

6. Toijem shear zone

In the Garpung Khola, not far from Toijem police station, at an altitude of 3300 m (Fig. 7), a nearly 50 m thick ductile shear zone (Toijem shear zone: TSZ) was recognized in the kyanite- and sillimanite-bearing gneisses of the HHC. The mylonites are localized at the top of the gneisses of Unit 1 near the contact with the overlying gneiss with abundant white mica and high metamorphic grade marbles of Unit 2. The TSZ, localized at the boundary between Units 1 and 2, does not cause a repetition of the units in the HHC in the study section.

Mylonites from the TSZ show augen and microlithons made by Grt, Pl, Qtz, Ky, and Ms. The mylonitic foliation is defined by Bt + Ms, Sil, Qtz and stretched plagioclase. Shear planes strike N110–120° and dip moderately to the NE (40–45°). Elongation and mineral lineation marked by tails around mm- to cm-size feldspar porphyroclasts of Grt Qtz, Sil, and Bt trend N45° and plunge 30–40° to the NE. The sense of shear deduced from shear band cleavages, mica fishes and rotated porphyroclasts, is top-to-the-SW (Fig. 13a and b). Sillimanite crystals occur along shear planes (Fig. 13c) and are more abundant with respect to the footwall of the TSZ where sillimanite is present only as small beards at the end of kyanite crystals. Very few small leucogranite bodies appears stretched within the shear zone.

This shear zone splits the HHC in two portions: a lower one and an upper one; stretched and folded leucogranite dikes and sills occur above the TSZ.

7. Tethyan zone

The lower part of the TSS is composed of impure limestone, calcschist, and quartzite of the Dhaulagiri Formation (Fig. 14) (Fuchs and Frank, 1970; Fuchs, 1977) characterised by the metamorphic assemblage Cc + Qtz + Ms + Bt ± Chl ± Scp, indicating greenschist facies condition (Garzanti et al., 1994; Schill et al., 2002; Carosi et al., 2002).

Three deformation phases have been recognized in the lower part of the TSS (Fig. 15). $D1_{TSS}$ phase is characterized by an $S1_{TSS}$ penetrative low-grade foliation affecting the sedimentary bedding S0, clearly recognizable both in the field and in thin section in the reddish metasandstones and quartzites (Fig. 14b). $S1_{TSS}$ foliation is axial plane of open to tight folds. It strikes mostly NW–SE and has variable dips from sub-horizontal to 80–85°, both toward the NE and the SW (Fig. 3) as a result of the later tectonic events. $S1_{TSS}$ is best developed in the more pelitic layers, where it assumes the characteristics of a continuous foliation. It is associated with the syn-kinematic crystallization of quartz, calcite, muscovite, biotite, chlorite, and oxides. In the more competent levels $S1_{TSS}$ is a spaced rough, or sometimes anastomosing, cleavage.

$D2_{TSS}$ deformation is characterized by a ubiquitous $S2_{TSS}$ cleavage, ranging from a continuous foliation to a crenulation (Fig. 16c). $S2_{TSS}$ foliation strikes NW–SE and dips mostly, from 20° to 40°, toward the NE (Fig. 3). $S2_{TSS}$ foliation is axial planar to asymmetrical $F2_{TSS}$ folds always showing a vergence toward the NE. $A2_{TSS}$ axes show variable orientations but they mostly trend NW–SE dipping a very few degrees toward the NW (Fig. 3).

Going upwards in the sequence $S2_{TSS}$ foliation is well-developed only in the pelitic levels, where it ranges from a zonal to a discrete crenulation cleavage. Only sometimes syn-kinematic re-crystallization of white mica has been observed.

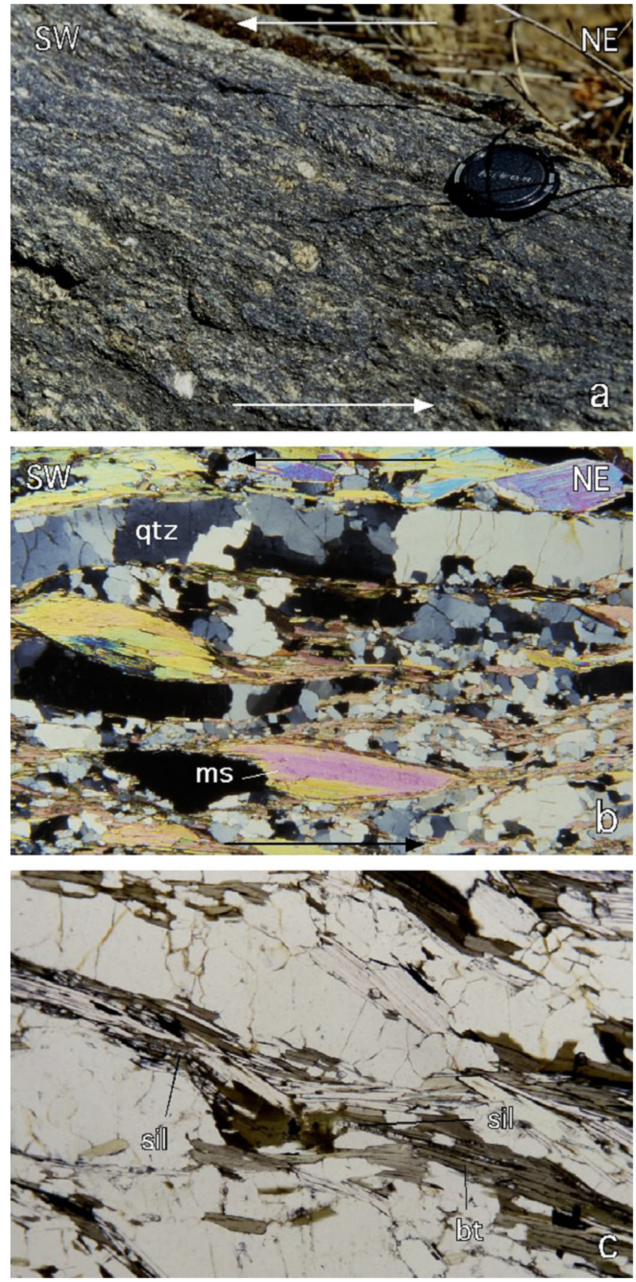

Fig. 13. Toijem Shear Zone (Garpung Khola valley). (a) Mylonite in garnet and sillimanite-bearing gneisses with sigma-type porphyroclasts; top-to the SW sense of shear. Lens cap for scale (5.2 cm); (b) mica fish and ribbon quartz in a mylonite from the TSZ; top-to the SW sense of shear. Crossed polars; field of view is 1.2 mm; (c) biotite and sillimanite on shear planes in the TSZ. Crossed polars; field of view is 1.1 mm.

$S2_{TSS}$ foliation is sometimes affected by an $S3_{TSS}$ crenulation cleavage axial plane of open and nearly upright folds (Fig. 15). NW–SE trending antiforms and synforms affect the tectonic units, as well as the STDS and MCT zone (Upreti, 1999) (Fig. 1b).

We can clearly observe the growth of mm-size biotite porphyroblasts and muscovite in the lower part of the TSS. Microstructural relations pointed out that their

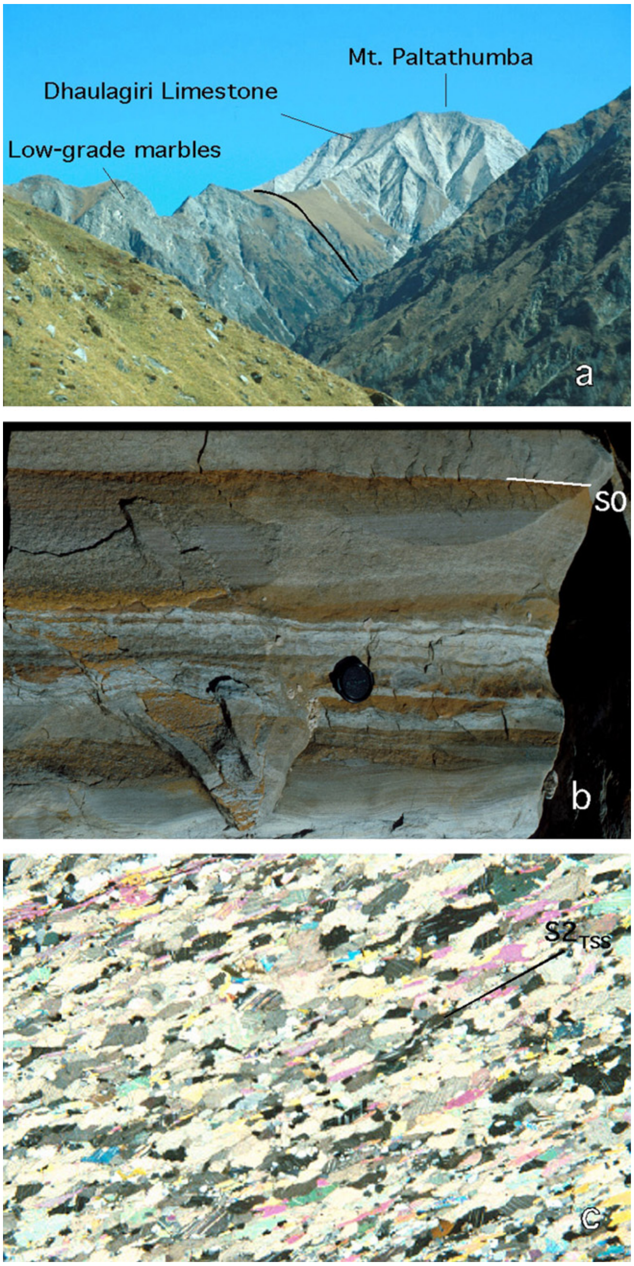

Fig. 14. (a) Dhaulagiri Limestone and low-grade marbles of the Tibetan Sedimentary Sequence (TSS) in the Panipatta Khola (Fig. 5); (b) sedimentary bedding (S0) in the Dhaulagiri Limestone near Kangmara La; (c) grain shape preferred orientation along $S2_{TSS}$ foliation in low-grade marbles at the base of the TSS. Crossed polars; field of view is 3.2 mm.

growth is post-S1 foliation and pre- to syn-S2 up to post-S2 (Fig. 16d). They testify to a LP–LT metamorphic event after the main $D1_{TSS}$ re-crystallization and metamorphism (Pognante and Benna, 1993).

Going from the upper portion of the TSS, in the Phoksundo Tal, down to the detachment zone we can observe an increase in metamorphic grade and a change from low temperature deformation mechanisms to crystalline plasticity in quartz and calcite with pervasive deformation (Fig. 14c). The $S2_{TSS}$ foliation progressively transposes

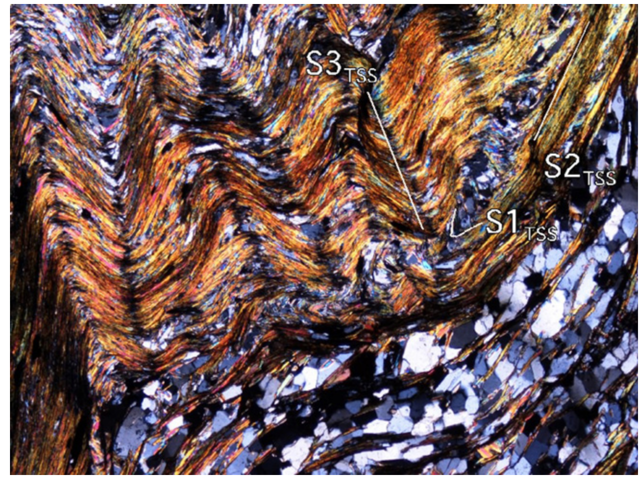

Fig. 15. Phyllite in the Tibetan Sedimentary Sequence (TSS) showing three ductile deformation phases: an earlier S1 low-grade foliation preserved in $S2_{TSS}$ microlithons, an $S2_{TSS}$ evoluted crenulation cleavage and a later spaced crenulation cleavage ($S3_{TSS}$) axial plane of open and mainly upright folds. Crossed polars; field of view is 3 mm.

the $S1_{TSS}$ foliation approaching the contact with the HHC. Metamorphic minerals progressively acquire a shape-preferred orientation parallel to the $S2_{TSS}$ foliation (Fig. 14c).

In the upper part of the TSS pressure solution deformation mechanisms predominate. It affects fossil shell valves as well as detrital grains; the foliation is here millimetre spaced. Approaching the marbles, foliation becomes pervasive and quartz and calcite grains accommodate deformation by crystal plasticity. Calcite deformation twins also indicate a downward increase in the temperature of deformation (Schill et al., 2002). In the detachment zone elongate ribbon calcite grains are observed. They show undulatory extinction, mechanical twins, and dynamic re-crystallization.

Leucogranite dykes and sills intruded the low-grade marble ranging from undeformed, to stretched and folded (Fig. 16a and b). They usually crosscut the $S1_{TSS}$ foliation and show complex relation with respect to the $D2_{TSS}$ deformation phase. The pattern of stretched, folded and rotated dykes allow recognizing a deformation field in agreement to a top-to-the-NE deformation related to the activity of the STDS (Carosi et al., 2002).

8. Discussion

8.1. Vorticity in the MCT zone

Mean vorticity values calculated in the MCT zone in Lower Dolpo range from 0.66 to 0.77, pointing to a non-coaxial regime of deformation as suggested by Vannay and Grasemann (2001) and Grasemann et al. (1999). Moreover, the present data are particularly interesting when compared to the available mean vorticity data in the HHC. Law et al. (2004) in the STDS in the Mt. Everest area obtained W_m values ranging between 0.67 and 0.98,

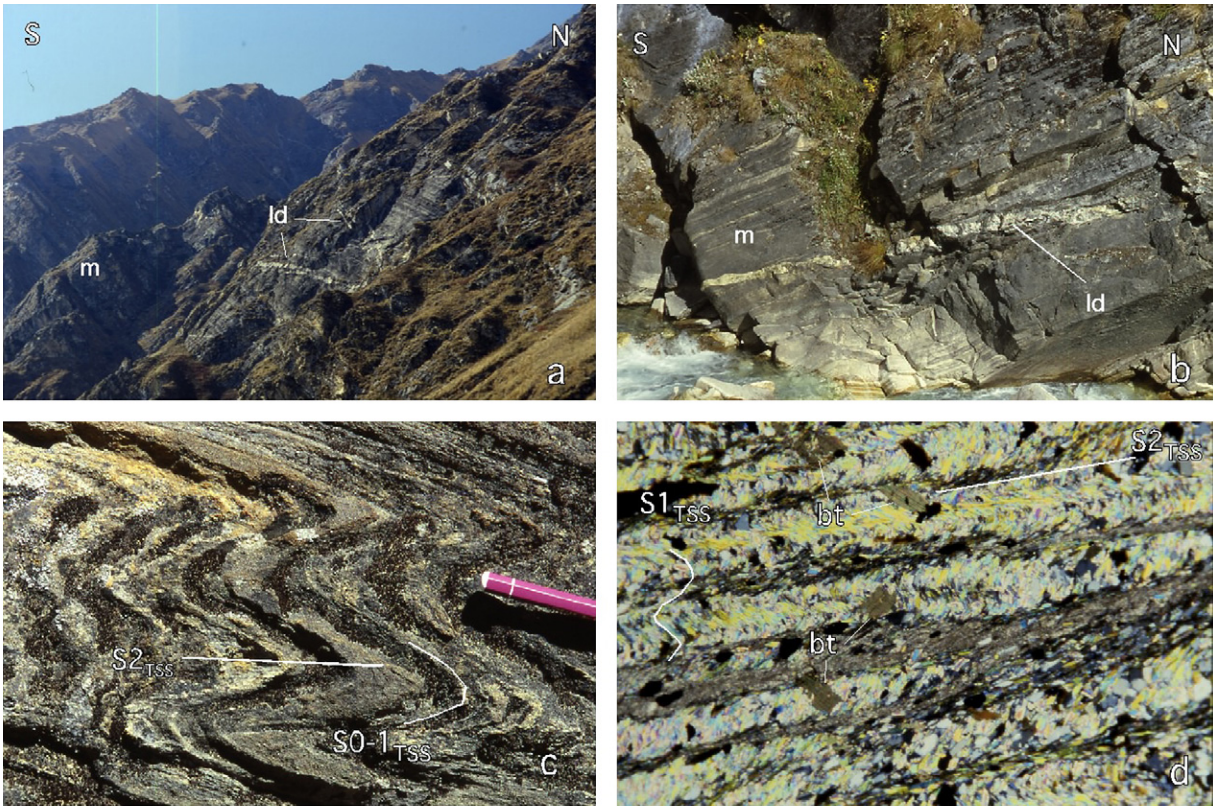

Fig. 16. Tibetan Sedimentary Sequence (TSS). (a) Panoramic view; (b) detail of outcrop (field of view is nearly 5 m) of low-grade marbles (m) intruded by leucogranite dykes (ld) at the base of the TSS in the Gorpung Khola; (c) asymmetric $F2_{TSS}$ folds in the TSS; pencil for scale; (d) thin section showing $S1_{TSS}$, $S2_{TSS}$ foliations in metapelites and growth of post-$S1_{TSS}$ and pre- to post $S2_{TSS}$ biotite porphyroblasts. Crossed polars, field of view is 1 mm.

pointing to a non-coaxial deformation with high percentage of simple shear.

On the other hand, data from Carosi et al. (2004a,b) in western Bhutan from the core of the HHC, confirm the non-coaxial regime of deformation with an important component of pure shear during deformation. Here, W_m values obtained by the same method (from 0.66 to a maximum of 0.76), indicate a pure shear-dominated deformation. Considering the W_m values and the tectonic position of the samples, the available W_m values indicate an increase in the simple shear component moving from the core to the boundaries of the extruding unit.

Moreover, this distribution of vorticity values across the HHC is in agreement with a ductile extrusion model as proposed by Grujic et al. (1996, 2002) and Law et al. (2004). It is also compatible with the ductile model of extrusion of a wedge bounded by non-parallel faults (see Hodges et al., 1993) because in this case also strain compatibility requires simple shear together with pure shear to accommodate the deformation.

8.2. Tectonics in the HHC

The HHC is regarded as a ductile wedge of crystalline rocks extruded by the contemporaneous activity of the STDS and MCT zone (Burchfiel et al., 1992; Hodges et al., 1993) or exhumed by a channel flow model (Grujic et al., 1996, 2002). The results from the study area highlight the evolution of both compressional and extensional structures from ductile to brittle, as we would expect to find in an exhuming crystalline unit rising from depth. Moreover, the presence of a ductile shear zone in the middle part of the HHC (TSZ) in between the STDS and MCT zones developed under high-temperature conditions and closely related to the emplacement of leucogranites, suggests its primary role in the exhumation and decompression of the unit. Sillimanite is present in the kyanite-bearing gneiss of Unit 1, but it is particularly abundant along the TSZ.

According to Pognante and Benna (1993), Lombardo et al. (1993), Carosi et al. (1999), Hodges et al. (1996), Hodges (2000 with references) and Borghi et al. (2003) the HHC underwent an Eo-Himalyan High P phase of metamorphism reaching kyanite grade followed by a Neo-Himalayan phase during which the HHC was decompressed and reached the sillimanite stability field. Temperature and pressure estimates in micaschists and gneisses confirm an early stage of relatively HP, reaching the kyanite stability field, in the nearby Annapurna range (Vannay and Hodges, 1996; Hodges et al., 1996; Godin et al., 2001).

The growth of sillimanite on shear planes in the TSZ can be explained by the fast decompression of the hanging wall of the TSZ, enhanced by its kinematics during the general extrusion of the HHC. If we add the observation that leucogranites are emplaced above the TSZ only, it is evident that the TSZ played a key role in decompressing the hanging wall where melt was generated and emplaced. These lines of evidence and the geometry and kinematics of the TSZ indicated that the hanging wall of the TSZ is the most decompressed portion of the HHC in the study area.

Ductile to brittle shear zones are common features in the HHC and they have been described in the middle and upper portion of the HHC in other areas of the belt such as in the Annapurna Range (Kalopani Shear Zone: Vannay and Hodges, 1996; Modi Khola Shear Zone; Hodges et al., 1996), in Langtang (Macfarlane, 1993), in the Mt. Everest region (Khumbu Thrust: Maruo and Kizaki, 1983; Searle, 1999), in the Arun Valley (Barun Thrust: Goscombe and Hand, 2000) and in Bhutan (Kakhtang Thrust: Grujic et al., 1996; Davidson et al., 1997). They are usually interpreted as syn- to post-metamorphic out of sequence thrusts, sometimes doubling the HHC sequence. Their age has been constrained at 22.5–18.5 in central Nepal (Hodges et al., 1996) and 15–13 Ma both in central Nepal and in Bhutan (Vannay and Hodges, 1996; Grujic et al., 2002).

However, Toijem high-grade shear zone with a top-to-the-SW sense of shear localized in between Units 1 and 2 (Figs. 1, 7, 17) in a particularly thin section of the HHC joined with its decompressive character could be related to the earlier stages of extrusion of the HHC or by channel

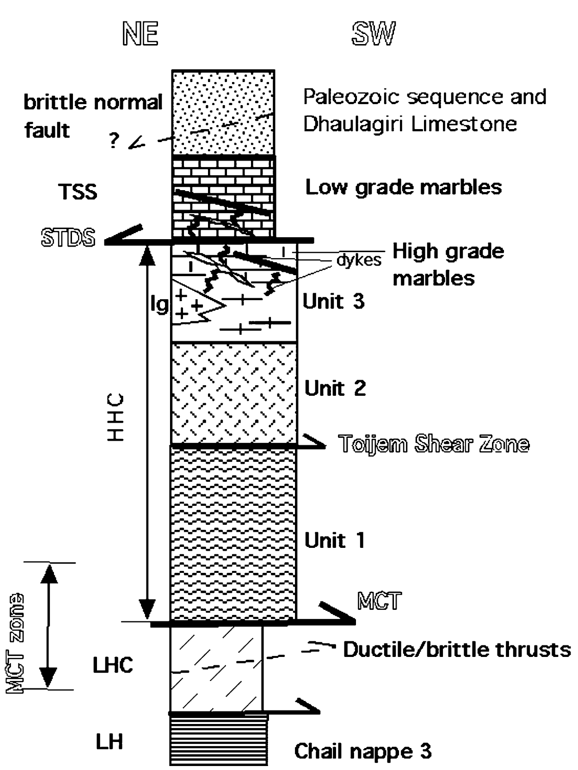

Fig. 17. Simplified sketch (not to scale) showing the localization of the main shear zones in the units of the study section. TSS, Tibetan Sedimentary Sequence; HHC, Higher Himalayan Crystalline; LHC, Lesser Himalayan Crystallines; LH, Lesser Himalaya sequence; MCT, Main Central Thrust; STDS, South Tibetan Detachment System: lg, leucogranites.

flow. In this latter case, the velocity profile during extrusion has not a perfect parabolic shape as in the ideal model (Grujic et al., 1996, 2002) but shows a perturbation (a break) corresponding to major changes in lithotype, such as the boundary between Units 1 and 2. This contact zone in the HHC could act as a zone of weakness localizing deformation and causing a step in the velocity field, with the hanging wall rocks moving relatively faster upward and southward with respect to the footwall (Fig. 18).

However, the presence of shear zones at the main boundaries among the three units in the HHC (TSZ; Kalopani Shear Zone: Vannay and Hodges, 1996; Modi Khola Shear Zone: Hodges et al., 1996) suggests that major lithological divisions had an influence in the localization of deformation during the extrusion of the HHC itself. Once deformation was localized and the hanging wall rocks began to move faster with respect to the footwall rocks, the relatively rapid decompression allowed the kyanite-bearing rocks of the hanging wall to reach the sillimanite stability field, with the generation and emplacement of melt.

8.3. The contact between TSS and HHC

The contact between the TSS and HHC is not as striking, because marbles, characterized by a different metamorphic grade, overlie marbles (Carosi et al., 2002). The biotite-bearing marbles of the TSS are brought into contact with the medium grade diopside-bearing marbles of the HHC. On the other hand, the LP–LT metamorphic event has the effect of obliterating the high-strain fabric of the shear zone, with the post-D2 growth of biotite. Only a few kinematic indicators are recognized in the study area, such as shear bands and a delta-type rotated pegmatite dyke intruded into the carbonate sequence, pointing to a top-to-the-northeast sense of shear (Carosi et al., 2002). The widespread development of D2 northeast-verging asymmetrical folds affecting the TSS, from mm- up to km-scale, is interpreted by several authors (Burchfiel et al., 1992; Burg et al., 1996; Carosi et al., 1998, 2002) to be related strictly to the top-to-the-NE normal high-strain zone.

A different interpretation has been proposed for the F2 north-verging asymmetrical folds in the TSS of the Annapurna Range by Brown and Nazarchuk (1993), Godin et al. (1999a,b, 2001), Searle and Godin (2003). They proposed a polyphase deformation history in which, after a top-to-the-SW Eo-Himalayan D1 phase, F2 folds developed in a compressional setting affecting both the TSS and the HHC. The Annapurna detachment, correlated with the STDS, developed later with respect to F2 folds during a D3 tectonic phase. This detachment transposed F2 folds into a high strain zone and deformed the attitude of their axial planes. A further shortening, characterized by kink folds (D4 phase), has been followed by brittle normal faults. The main difference between the two interpretations lies in the tectonic setting of the F2 asymmetrical folds localized at

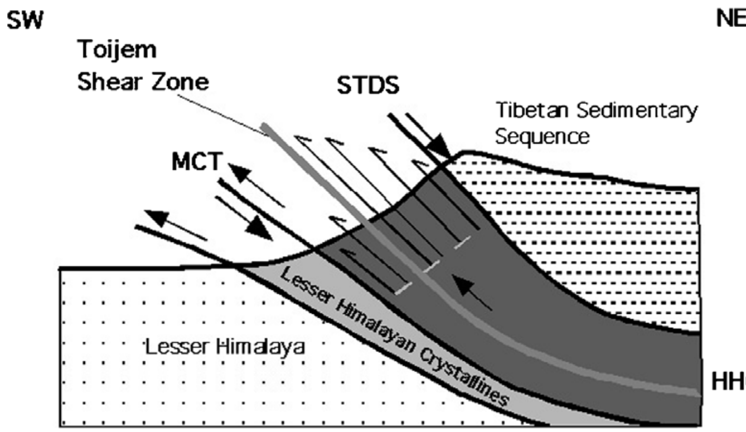

Fig. 18. Hypothesized sketch of velocity profile in the extruding Higher Himalayan Crystallines (HHC) with the presence of top-to-the SW high-grade Toijem Shear Zone causing a 'break' in the velocity profile. All the points in the HHC were extruded southward, but the points in the hanging wall of the TSS moved faster with respect to the points in the footwall as consequence of the activity of the ductile shear zone. The faster velocity of extrusion in the hanging wall of the Toijem Shear Zone, coupled with the activity of the STDS, enhanced its decompression with respect to the footwall. The figure has been redrawn and modified after R. Holcombe and M. Hand (Web page of Continental Evolution Research Group, University of Adelaide, Australia).

the base of the TSS. Anyway, the problem is still open to interpretation, since we did not find evidence in the Dolpo transect supporting completely the shortening or compressive origin of F2 folds, as proposed by Godin et al. (1999a).

Moreover there are some observations that must be taken into consideration:

1. In the high-strain zone towards the base of the TSS we observed an increasing $D2_{TSS}$ strain giving rise to a more and more penetrative $S2_{TSS}$ axial plane foliation and tighter $F2_{TSS}$ folds. Moreover, we did not find at the microscale, structural evidence for an overprint by a mylonitic fabric of the D3 high-strain zone onto the $S2_{TSS}$ foliation. In our thin sections the $D2_{TSS}$ deformation phase is developed ubiquitously, and it can be observed from the less deformed upper portion of the TTS down to the high strain zone. If the high-strain zone developed well after $F2_{TSS}$ folds and $S2_{TSS}$ foliation we should expect to find a transposition, with relics of the $S1_{TSS}$ and $S2_{TSS}$ foliations in less strained areas. It is unlikely that the D3 high-strain zone could have completely obliterated any microstructural evidence of the $D2_{TSS}$ foliation, or have been superposed on it, so that they were exactly parallel. In addition to this, $D1_{TSS}$ and $D2_{TSS}$ deformations are easily detectable at the microscale and give rise to penetrative foliations. On the contrary, the $S3_{TSS}$ foliation is linked to quite open folds, with geometry suggesting only a little amount of shortening, and it is unlikely that it could be related to the formation of a high-strain shear zone.

2. Godin et al. (1999a,b) reported a 'drag effect' by the D3 high-strain zone on the $S2_{TSS}$ axial plane foliation to explain the northward dip of the $S2_{TSS}$ foliation. The north-dipping foliation could be explained as well as by the D3 antiforms and synforms affecting the whole nappe pile and the MCT and STDS as described in this paper (Fig. 1b). The geological cross section in the Jumla area by Upreti (1999; Fig. 9) clearly shows the folding of the MCT and STDS by upright antiforms and synforms.

3. Even if it is difficult to observe a perfect cylindrical development of the belt all along its strike we have to take into an account the presence of different metamorphic paths in the HHC and in the overlying TSS. From this point of view the compressive setting for the D2 fan structure proposed by Godin et al. (1999a,b, 2001) for both the TSS and the HHC at the same structural level, before the extrusion of the HHC itself, seems to be problematic when considering the different metamorphism recorded in the two units. Pognante et al. (1993), Pognante and Benna (1993), Lombardo et al. (1993) and Guillot et al. (1999 with references) reported significantly different PTt paths for the two units. Moreover, the pressure reached by the HHC was much higher with respect to that of the TSS in the Eo-Himalayan phase, especially when considering the presence of granulites and eclogites in the HHC, both to the west and to the east (Pognante and Spencer, 1991; Guillot, 1999; Guillot et al., 1995, 1999; Carosi et al., 1999; Lombardo and Rolfo, 2000; Borghi et al., 2003). In the light of these data the overthickening of the TSS by the growth of the D2 fan structure (nearly 25 km) is not enough to produce the required pressure for generation of granulites and eclogites in the underlying HHC.

According to our data the boundary between the TSS and the HHC has a different position compared with the position mapped by previous authors. The crystalline marbles mapped by Fuchs and Frank (1970) and Fuchs (1977) have been divided in two parts and have been attributed to two different tectonic units: the lower part, showing an amphibolite facies calc-silicate assemblages, is attributed to the HHC, whereas the upper portion, underlying the Dahulagiri Limestone, with greenschist facies metamorphism is attributed to the TSS. The latter portion can be tentatively correlated with the North Col Formation cropping out in the Mt. Everest area above the lower ductile extensional shear zone of the STDS (Pognante and Benna, 1993; Carosi et al., 1998; Carosi et al., 2002) or to the

Checka Formation cropping out in Bhutan (Gansser, 1983; Grujic et al., 1996) as they show the same geometrical position, metamorphic grade and structural and lithologic features. The lower portion of the crystalline marbles can be correlated with the Larjung Formation in the Kali Gandaki, regarded by Vannay and Hodges (1996) as part of the HHC (Carosi et al., 2002).

The Low P and Low T metamorphic event giving rise to the static growth of muscovite and biotite porphyroblasts on $S1_{TSS}$ and $S2_{TSS}$ foliations at the base of the TSS is not restricted to the Dolpo region. This feature has been recognized all over the Himalayan Belt since the beginning of Himalayan researches. This metamorphic event is present also in the Bhudi Schist of Kumaon (Heim and Gansser, 1939), in the North Col Formation in the Cho Oyu-Everest-Makalu area (Pognante and Benna, 1983; Lombardo et al., 1993; Carosi et al., 1999) and in the Chekha Formation in Bhutan (Gansser, 1983). This widespread occurrence suggests a regional control on its development rather than purely a local effect. Both HHC and TSS tectonic units underwent different PTt paths with very different maximum PT conditions during the metamorphic climax in the Eo-Himalayan stage (Garzanti et al., 1994; Pognante and Benna, 1993; Lombardo et al., 1993; Vannay and Hodges, 1996; Carosi et al., 1999; Hodges, 2000).

If we consider the underthrusting and subsequent extrusion of the HHC, it is clear that the contact with the overlying TSS changed during time, with different relationships and was in contact with different portions of the two units throughout time. However, the actual extensional contact (STDS) was formed during the phase of extrusion of the HHC (23–17 Ma; Hodges, 2000). At this stage 'hot rocks' in the amphibolite facies (sillimanite grade), with migmatites and the development and emplacement of leucogranites in the upper part of the HHC, were brought into contact with the lower metamorphic grade rocks of the base of the TSS. The different temperatures of adjacent units caused conductive heating from the HHC to the TSS. Heat transfer from HHC to TSS developed in close relationship with extensional deformation, as testified by the relationship between the growth of biotite porphyroblasts and the $S2_{TSS}$ foliation. Static growth of biotite porphyroblasts after the $S2_{TSS}$ foliation suggests that heating continued after ductile deformation ceased.

Another constraint on the timing of the contact between the TSS and the HHC is the striking presence of a network of leucogranite dykes and sills in the metamorphic unit at the base of the TSS. Even if their emplacement history is quite complex, they originated from the HHC and they usually crosscut the $S1_{TSS}$ fabric and are deformed by the following phases, suggesting that they were able to intrude the upper tectonic unit only after the $D1_{TSS}$ deformation phase.

Eo-Himalayan metamorphism is linked to the first tectonic phase (Pognante and Benna, 1993; Garzanti et al., 1994; Schill et al., 2002; Crouzet et al., 2003) whereas the Neo-Himalayan stage developed after it, from syn- to post-D2. In our reconstruction the top-to-the NE asymmetrical folds at the base of the TSS are linked to STDS, i.e., when the higher-grade rocks of the HHC were in contact with the upper lower grade rocks of the TSS.

9. Conclusions

Geological and structural studies in the Lower Dolpo transect, cutting across three of the main tectonic units of the Himalayan belt (LHC, HHC, and TSS) highlight the following tectonic and metamorphic features:

(1) Mean vorticity values point to non-coaxial flow in the MCT zone, in agreement with the distribution of vorticity that we could be expected during the ductile extrusion of a wedge in which the pure shear component enhances the extrusion of the unit;

(2) The HHC shows a highly reduced thickness with respect to sections in eastern Nepal, particularly in the uppermost portion, and it is characterized by a high-temperature compressional shear zone (Toijem SZ) localized between Units 1 and 2;

(3) The high-temperature TSZ (sillimanite grade) could have been developed during the early stages of extrusion of the HHC, pointing to an heterogeneous velocity path in which the hanging wall of the TSZ moved faster upward and southward with respect to the footwall rocks. This also suggests that major lithological breaks (such as the boundaries among Units 1, 2, and 3) exerted a strong influence during extrusion of the whole HHC, allowing the concentration of deformation and affecting the velocity of the extruded units;

(4) The STDS is responsible for the jump in metamorphic grade passing from biotite-bearing marble at the base of the TSS to the underlying diopside-bearing marble of the HHC. Both marbles show final low-temperature deformation but the former arrived at this stage by a prograde path, whereas the latter arrived at this stage after the metamorphic peak in the amphibolite facies, and were only later retrogressed under greenschist facies conditions;

(5) In the TSS, the strain increases toward the boundary between HHC and TSS. Deformation mechanisms changed from pressure solution to crystalline plasticity going down from Ordovician limestone to the marbles below the Dhaulagiri Limestone;

(6) The TSS is characterized by widespread F2 asymmetric folds with a north-eastern vergence due to the activity of the STDS affecting a previous continuous foliation developed under low-grade metamorphic conditions during the Eo-Himalayan phase;

(7) The base of the TSS is affected by a LP metamorphic event, due to conductive heating from the hotter HHC.

(8) Large scale folding, after the STDS, affects the TSS and the whole nappe pile causing the formation of wide antiforms and synforms that after erosion gives rise to HHC and TSS wide outliers above the LH.

Acknowledgement

Fieldwork in western Nepal was financially supported by National Research Council of Italy (IGG) and Funds from the University of Pisa and Padova. We wish to thank S. Guillot and L. Godin for constructive criticism.

References

Arita, K., 1983. Origin of the inverted metamorphism of the Lower Himalayas. Central Nepal. Tectonophysics 93, 43–60.

Borghi, A., Castelli, D., Lombardo, B., Visonà, D., 2003. Thermal and baric evolution of garnet granulites from the Kharta region of S. Tibet, E. Himalaya. European Journal of Mineralogy 15, 401–418.

Brown, R.L., Nazarchuk, J.H. 1993. Annapurna detachment fault in the Greater Himalaya of central Nepal. In: Treloar, P.J., Searle, M.P. (Eds.), Himalayan Tectonics. Geological Society of London Special Publication 74, 461-473.

Burchfiel, B.C., Chen, Z., Hodges, K.V., Liu, Y., Royden, L.H., Changrong, D., Xu, L., 1992. The South Tibetan Detachment System, Himalayan Orogen: extension contemporaneous with and parallel to shortening in a collisional mountain belt. Geological Society of American Special Paper 269, 41.

Burchfiel, B.C., Royden, L.H., 1985. North-south extension within the convergent Himalayan region. Geology 13, 679–682.

Bureau of Geology and Mineral Resources of Xizang Autonomous Region, 1993. Regional geology of Xizang (Tibet) Autonomous Region. People's Republic of China, Ministry of Geology and Mineral Resources, Geological Memoirs Series 1, 31, Geological Publishing House, Beijing, 707 p. (in Chinese, with English summary).

Burg, J.P., Brunel, M., Gapais, D., Chen, G.M., Liu, G.H., 1984. Deformation of leucogranites of the crystalline main central thrust sheet in southern Tibet (China). Journal of Structural Geology 6, 535–542.

Burg, J.P., Chaudry, M.N., Ghazanfar, M., Anczkiewicz, R., Spencer, D., 1996. Structural evidence for the backsliding of the Kohistan arc in the collisional system of northwest Pakistan. Geology 24, 739–742.

Caby, R., Pêcher, A., Le Fort, P., 1983. Le grand chevauchement central himalayen: nouvelles données sur le métamorphisme inverse à la base de la Dalle du Tibet. Revue Géologie Dynamique Géographie Physique 24, 89–100.

Carosi, R., Lombardo, B., Molli, G., Musumeci, G., Pertusati, P.C., 1998. The South Tibetan Detachment System in the Rongbuk valley, Everest region. Deformation features and geological implications. Journal of Asian Earth Science 16, 299–311.

Carosi, R., Lombardo, B., Musumeci, G., Pertusati, P.C., 1999. Geology of the Higher Himalayan Crystallines in Khumbu Himal (Eastern Nepal). Journal of Asian Earth Science 17, 785–803.

Carosi, R., Montomoli, C., Visonà, D., 2002. Is there any detachment in the Lower Dolpo (western Nepal)? Comptes Rendus Geoscience 334, 933–940.

Carosi, R., Montomoli, C., Visonà, D., 2004a. Extensional shear zones in the core of higher Himalayan Crystallines (Bhutan Himalaya): evidence for extrusion? Abstract. In: Channel flow, ductile extrusion and exhumation of lower-mid crust in continental collision zones. Londra 2004, 13.

Carosi, R., Montomoli, C., Visonà, D., 2004. Deformation features of the Higher Himalayan Crystallines in Western Bhutan during exhumation. Abstract. In: 19th Himalayan–Karakoram–Tibet workshop, Niseko, Hokkaido, Japan 2004. Himalayan Journal of Sciences 2(4), 108.

Catlos, E.J., Harrison, T.M., Dubey, C.S., Edwards, M.A., 2002. P–T-t constraints on the evolution of the Sikkim Himalaya. Abstract Journal of Asian Earth Science 20 (4A), 6–7.

Catlos, E.J., Dubey, C.S., Harrison, T.M., Edwards, M.A., 2004. Late Miocene movement within the Himalayan Main Central Thrust shear zone, Sikkim, north-east India. Journal of Metamorphic Geology 22, 207–226.

Chemenda, A.I., Mattauer, M., Malavieille, J., Bokun, A.N., 1995. A mechanism for syn-Collisional deep rock exhumation and associated normal faulting: results from physical modeling. Earth and Planetary Science Letters 132, 225–232.

Coleman, M.E., 1996. Orogen-parallel and orogen-perpendicular extension in the central Nepalese Himalayas. Geological Society of American Bullettin 108, 1594–1607.

Crouzet, C., Gautam, P., Schill, E., Appel, E., 2003. Multicomponent magnetization in western Dolpo (Tethyan Himalaya, Nepal): tectonic implications. Tectonophysics 377, 179–196.

Daniel, C.G., Hollister, L.S., Parrish, R.R., Grujic, D., 2003. Exhumation of the Main Central Thrust from Lower Crustal Depths, Eastern Bhutan Himalaya. Journal of Metamorphic Geology 21, 317–334.

Davidson, C., Grujic, D.E., Hollister, L.S., Schmid, S.M., 1997. Metamorphic reactions related to decompression and synkinematic intrusion of leucogranite, High Himalayan Crystallines, Bhutan. Journal of Metamorphic Geology 15, 593–612.

DeCelles, P.G., Robinson, D.M., Quade, J., Ojha, T.P., Garzione, C.N., Copeland, P., Upreti, B.N., 2001. Stratigraphy, structure, and tectonic evolution of the Himalayan fold-thrust belt in western Nepal. Tectonics 20, 487–509.

Edwards, M.A., Kidd, W.S.F., Li, J., Yue, Y., Clark, M., 1996. Multistage development of the southern Tibet detachment system near Khula Kangri: New data from Gonta La. Tectonophysics 260, 1–19.

Edwards, M.A., Pecher, A., Kidd, W.S.F., Burchfiel, B.C., Royden, L.H., 1999. Southern Tibetan Detachment System at Khula Kangri, eastern Himalaya: a large-area, shallow detachment stretching into Bhutan? Journal of Geology 107, 311–623.

Fuchs, G., 1964. Beitrag zur Kenntnis des Palaozoikums und Mesozoikums der tibetischen Zone in Dolpo (Nepal Himalaja). Sonderabdruck aus den Verhandlungen der Geologischen Bundesanstalt 1, 6–9.

Fuchs, G., 1977. The geology of the Karnali and Dolpo regions, Western Nepal, Jahrbuch der Geologischen Bundesanstalt Wien. Band 120 (2), 165–217.

Fuchs, G., Frank, W., 1970. The geology of West Nepal between the rivers Kali Gandaki and Thulo Bheri, Jahrbuch der Geologischeen Bundesanstalt. Sonderband 18, 3–103.

Gansser, A., 1964. Geology of the Himalayas. Interscience Publishers, London.

Gansser, A., 1983. Geology of the Bhutan Himalaya. Denkschriften der Schweizerischen Naturforschenden Gesellschaft 96. Birkhäiuser Verlag, Basel, 181 pp..

Garzanti, E., 1999. Stratigraphy and sedimentary history of the Nepal Tethys Himalaya passive margin. Journal of Asian Earth Science 17, 805–827.

Garzanti, E., Gorza, M., Martellini, L., Nicora, A., 1994. Transition from diagenesis to metamorphism in the Paleozoic to Mesozoic succession of the Dolpo-Manang Synclinorium and Thakkola Graben (Nepal Tethys Himalaya). Eclogae Geologicae Helveticae 87 (2), 613–632.

Godin, L., Brown, R.L., Hanmer, S., Parrish, R.R., 1999a. Backfolds in the core of the Himalyan orogen: an alternative interpretation. Geology 27, 151–154.

Godin, L., Brown, R.L., Hanmer, S., 1999b. High strain zone in the hanging wall of the Annapurna detachment, central Nepal Hiamalya. In: Himalaya and Tibet: Mountain roots to mountain tops. In: Macfarlane, A.M., Sorkhabi, R., Quade, J. (Eds.), Geological Society of America Special Paper 328, 199–210.

Godin, L., Parrish, R.R., Brown, R.L., Hodges, K.V., 2001. Crustal thickening leading to exhumation of the Himalayan metamorphic core of central Nepal: insight from U–Pb geochronology and $^{40}Ar/^{39}Ar$ thermochronology. Tectonics 20, 729–747.

Goscombe, B., Hand, M., 2000. Contrasting P–T Paths in the Eastern Himalaya, Nepal: inverted Isograds in a Paired Metamorphic Mountain Belt. Journal of Petrology 41 (12), 1673–1719.

Ghosh, S.K., Ramberg, H., 1976. Reorientation of inclusions by combination of pure shear and simple shear. Tectonophysics 34, 1–70.

Grasemann, B., Fritz, H., Vannay, J.C., 1999. Quantitative kinematic flow analysis from the Main Central Thrust Zone (NW-Himalaya, India); implications for a decelerating strain path and the extrusion of orogenic wedges. Journal of Structural Geology 21, 837–853.

Grujic, D., Casey, M., Davidson, C., Hollister, L., Kundig, K., Pavlis, T., Schmid, S., 1996. Ductile extrusion of the Higher Himalayan crystalline in Bhutan: evidence from quartz microfabrics. Tectonophysics 260, 21–43.

Grujic, D., Hollister, L., Parrish, R.R., 2002. Himalayan metamorphic sequence as an orogenic channel: insight from Bhutan. Earth and Planetary Science Letters 198, 177–191.

Guillot, S., 1999. An overview of the metamorphic evolution in Central Nepal. Journal of Asian Earth Sciences 17, 713–725.

Guillot, S., Cosca., M., Allemand, P., Le Fort, P., 1999. Contrasting metamorphic and geochronologic evolution along the Himalayan belt. In: Macfarlane, A.M., Sorkhabi, R., Quade, J. (Eds.), Himalaya and Tibet: Mountain roots to mountain tops. Special Paper 328, Geological Society of America, 177–128.

Guillot, S., Lardeaux, J.M., Mascle, G., Colchen, M., 1995. Un nouveau témoine du métamorphisme de haute-pression dans la chaîne himalayenne (Dôme du Tso Morari, east Ladakh). Paris Académie des Sciences, Comptes Rendues 320, 931–936.

Harrison, T.M., Ryerson, F.J., Le Fort, P., An Yin, Lovera, O.M., Catlos, E.J., 1997. A late Miocene origin for the central Himalayan inverted metamorphism. Earth and Planetary Science Letters 146, E1–E7.

Heim, A., Gansser, A., 1939. Central Himalaya. Geological observations of the Swiss Expedition 1936. Mémoires de la Société Helvétique des Sciences Naturelles 7/31, 245.

Hodges, K., 2000. Tectonics of Himalaya and southern Tibet from two perspectives. Bulletin of the Geological Society America 112, 324–350.

Hodges, K.V., Burchfiel, B.C., Royden, L.H., Chen, Z., Liu, Y., 1993. The metamorphic signature of contemporaneous extension and shortening in the central Himalayan orogen: data from the Nyalam transect, southern Tibet. Journal of Metamorphic Geology 11, 721–737.

Hodges, K.V., Parrish, R.R., Searle, M.P., 1996. Tectonics of the central Annapurna Range, Nepalese Himalayas. Tectonics 15, 1264–1291.

Kretz, R., 1983. Symbols for rock-forming minerals. American Mineralogist 68, 277–279.

Law, R.D., Searle, M.P., Simpson, R.L., 2004. Strain, deformation temperatures and vorticity of flow at the top of the Greater Himalayan Slab, Everest Massif, Tibet. Journal of the Geological Society, London 161, 305–320.

Le Fort, P., 1971. Les formations cristallophyliennes de la Thakkhola. Recherches géologiques dans l'Himalaya du Népal, région del Thakkhola, Édition du CNRS Paris.

Le Fort, P., 1975. Himalaya: the collided range. American Journal of Science 275A, 1–44.

Lombardo, B., Pertusati, P.C., Borghi, S., 1993. Geology and tectonomagmatic evolution of the eastern Himalaya along Chomolungma-Makalu tansect. In: Treloar, P.J., Searle M.P. (Eds.), Himalayan Tectonics. Geological Society of London Special Publication 74, 341–355.

Lombardo, B., Rolfo, F., 2000. Two contrasting eclogite types in the Himalayas: implications for the Himalayan orogeny. Journal of Geodynamics 30, 37–60.

Macfarlane, A.M., 1993. Chronology of tectonic events in crystalline core of the Himalaya, Langtang National Park, central Nepal. Tectonics 12 (4), 1004–1025.

Maruo, Y., Kizaki, K., 1983. Thermal structure in the nappes of the eastern Nepal Himalayas. In: Shams, F.A. (Ed.), Granites of Himalayas, Karakorum and Hindu Kush. Institute of Geology, Punjab University, Lahore, pp. 271–286.

Mu, A.T., Wen, S.H., Wang, Y.K., Chang, P.K., Yin, C.H., 1973. Stratigraphy of the Mount Jolmo Lungma region in Southern Tibet, China. Scientia Sinica 16, 96–111.

Passchier, C.W., 1987. Stable position of rigid objects in non-coaxial flow: study in vorticity analysis. Journal of Structural Geology 9, 679–690.

Passchier, C.W., Trouw, R.J., 1996. Microtectonics. Springer Verlag, Berlin, Heidelberg, 289.

Paudel, L.P., Arita, K., 2000. Tectonic and polymetamorphic history of the Lesser Himalaya in central Nepal. Journal of Asian Earth Sciences 18, 561–584.

Pognante, U., Benna, P., 1993. Metamorphic zonation, migmatization, and leucogranites along the Everest transect of Eastern Nepal and Tibet: record of an exhumation history. In: Treloar, P.J., Searle M.P. (Eds.), Himalayan Tectonics. Geological Society, London, Special Publicatio 74, 328–340.

Pognante, U., Benna, P., Le Fort, P. 1993. High-pressure metamorphism in the High Himalayan Crystallines of the Stak valley, northeastern Nanga Parbat-Haramosh syntaxis, Pakistan Himalaya. In: Treloar, P.J., Searle, M.P. (Eds.), Himalayan Tectonics. Geological Society of London Special Publication 74, 161-172.

Pognante, U., Spencer, D.A., 1991. First record of eclogites from the High Himalayan Belt, Kaghan valley (northern Pakistan). European Journal of Mineralogy 3, 613–618.

Robinson, D.M., De Celles, P.G., Garzione, C.N., Pearson, O.N., Harrison, T.M., Catlos, E.J., 2003. Kinematic model for the Main Central thrust in Nepal. Geology 31, 339–362.

Schill, E., Appel, E., Gautam, P., 2002. Towards pyrrhotite/magnetite geothermometry in low-grade metamorphic carbonates of the Tethyan Himalayas (Shiar Khola, central Nepal). Journal of Asian Earth Science 20, 195–201.

Searle, M.P., 1999. Extensional and compressional faults in the Everest-Lhotse massif, Khumbu Himalaya, Nepal. Journal of the Geological Society, London 156, 227–240.

Searle, M.P., Godin, L., 2003. The South Tibetan Detachment System and the Manaslu leucogranite: a structural reinterpretation and restoration of the Annapurna-Manaslu Himalaya, Nepal. Journal of Geology 111, 505–524.

Takagi, H., Kazunori, A., Takashi, S., Kobayashi, K., Awaji, D., 2003. Kinematic history of the Main Central Thrust zone in the Langtang area, Nepal. Tectonophysics 366, 151–163.

Upreti, B.N., 1999. An overview of the stratigraphy and tectonics of the Nepal Himalaya. Journal of Asian Earth Science 17, 577–606.

Vannay, J.V.C., Grasemann, B., 2001. Himalayan inverted metamorphism and syn-convergence extension as a consequence of a general shear extrusion. Geological Magazine 138, 253–276.

Vannay, J.C., Hodges, K., 1996. Tectonometamorphic evolution of the Himalayan metamorphic core between the Annapurna and Dhaulagiri, central Nepal. Journal of Metamorphic Geology 14, 635–656.

Wallis, R.S., 1992. Vorticity analysis in a metachert from the Sanbagawa Belt, SW Japan. Journal of Structural Geology 14, 271–280.

Wallis, R.S., 1995. Vorticity analysis and recognition of ductile extension in the Sanbagawa Belt, SW Japan. Journal of Structural Geology 17, 1077–1093.

Wallis, R.S., Platt, J.P., Knott, S.D., 1993. Recognition of syn-convergence extension in the accretionary wedges, with examples from the Calabrian arc and the Eastern Alps. American Journal of Science 293, 463–495.

Watts, D.R., Harris, N.B.W., the 2002 NASA GLENN Soars Working Group, 2005. Mapping granite and gneiss in domes along the North Himalayan antiform with ASTER SWIR band ratios. Geological Society of American Bulletin 117, 879–886.